Original article

MOLECULAR METABOLISM

TMEM135 deficiency improves hepatic steatosis by suppressing CD36 in a SIRT1-dependent manner

Arun Chhetri[1], Channy Park[1], Hyunsoo Kim[1], Laxman Manandhar[1], Chagtsalmaa Chuluunbaatar[1], Jaetaek Hwang[1], Xiaofan Wei[1], Gyuho Jang[1], Batching Chinbold[1], Hyug Moo Kwon[2], Sang-wook Lee[3], Raekil Park[1,*]

ABSTRACT

Objectives: Dysregulation of lipid homeostasis pathway causes many liver diseases, including hepatic steatosis. One of the primary factors contributing to lipid accumulation is fatty acid uptake by the liver. Transmembrane protein 135 (TMEM135), which exists in mitochondria and peroxisomes, participates in intracellular lipid metabolism. This study aims to investigate the role of TMEM135 on regulating cellular lipid import in the liver.

Methods: We used *in vivo, ex vivo*, and *in vitro* models of steatosis. TMEM135 knockout (TMEM135KO) and wild type (WT) mice were fed a high-fat diet (HFD) to induce hepatic steatosis. Primary mouse hepatocytes and AML12 cells were treated with free fatty acid (FFA). Additionally, TMEM135-deficient stable cells and overexpressed cells were established using AML12 cells.

Results: TMEM135 deficiency mitigated lipid accumulation in the liver of HFD-fed TMEM135KO mice. TMEM135-depleted primary hepatocytes and AML12 cells exhibited less lipid accumulation when treated with FFA compared to control cells, as shown as lipid droplets. Consistently, the effect of TMEM135 depletion on lipid accumulation was completely reversed under TMEM135 overexpression conditions. CD36 expression was markedly induced by HFD or FFA, which was reduced by TMEM135 depletion. Among the SIRT family proteins, only SIRT1 expression definitely increased in the liver of HFD-fed TMEM135KO mice along with a significant increase in NAD^+/NADH ratio. However, inhibition of SIRT1 in TMEM135-depleted cells using siSIRT1 or the SIRT1 inhibitor EX-527 resulted in an increase of CD36 expression and consequent TG levels.

Conclusions: TMEM135 depletion attenuates CD36 expression in a SIRT1-dependent manner, thereby reducing cellular lipid uptake and hepatic steatosis.

Keywords TMEM135; Lipid accumulation; CD36; SIRT1

1. INTRODUCTION

Transmembrane protein 135 (TMEM135), also known as peroxisomal membrane protein 52 (PMP52), is present in the outer membrane of mitochondria, peroxisomes and lipid droplets (LDs) [1–4]. Previous studies propose a key role of TMEM135 in mitochondrial dynamics and peroxisome abundance [1,4]. TMEM135 is also known to be involved in the longevity and lipid accumulation of worms [2]. $TMEM135^{FUN025/FUN025}$, TMEM135 mutant mice increase lipid accumulation in retinal pigmented epithelium [5]. Recently, $TMEM135^{FUN025/FUN025}$ mice, which have increased peroxisome number and beta-oxidation, were shown to be protected against the development of fatty liver [1].

Lipid homeostasis in the liver is controlled through several molecular mechanisms, including fatty acid (FA) uptake, de novo lipogenesis, FA oxidation (FAO) and very-low-density lipoprotein secretion [6]. Dysregulation in any of these pathways leads to lipid accumulation in the liver [6]. Increased uptake of free FA (FFA) and lipoproteins from blood circulation is one of the major factors for hepatic lipid accumulation in patients with metabolic dysfunction-associated steatotic liver disease (MASLD) [7]. FA uptake in the liver is predominantly dependent on FA importers with a negligible contribution from passive diffusion [6]. Cluster differentiation 36 (CD36, fatty acid translocase), fatty acid transport protein (FATP), and caveolins are major FA transporters in the liver [6].

CD36 is a transmembrane protein, a member of the family of class B scavenger receptors, also known as scavenger receptor B2 (SR-B2), and facilitates the uptake of oxidized low-density lipoprotein and FA, with a high affinity for long-chain fatty acids [8,9]. Among the various FA transporters, CD36 is the most efficient transporter known to date [10]. Although expressed at low levels in normal hepatocytes, hepatic CD36 expression positively correlates with the development of hepatic

[1]Department of Biomedical Science and Engineering, Gwangju Institute of Science and Technology, Gwangju 61005, Republic of Korea [2]School of Life Sciences, Ulsan National Institute of Science and Technology, Ulsan, Republic of Korea [3]Department of Radiation Oncology Asan Medical Center, Seoul, Republic of Korea

*Corresponding author. Department of Biomedical Science & Engineering, Gwangju Institute of Science and Technology, Gwangju 61005, Republic of Korea. E-mail: rkpark@gist.ac.kr (R. Park).

Received September 5, 2024 • Revision received November 19, 2024 • Accepted November 28, 2024 • Available online 9 December 2024

https://doi.org/10.1016/j.molmet.2024.102080

steatosis [11]. Its role in FA uptake is evident in CD36-null mice that have impaired cellular FA uptake, an inability for lipid accumulation in the tissues and are resistant to diet-induced obesity [12]. CD36 is transcriptionally activated by peroxisome proliferator activated receptor-gamma (PPAR-γ), liver X receptor (LXR), and pregnane X receptor (PXR) [13]. Moreover, SIRT1 plays a pivotal role in regulating CD36 expression [14–17].

SIRTUIN 1 (SIRT1) is a NAD^+ dependent deacetylase that regulates many metabolic processes. SIRT1 has a protective role against MASLD which makes it an attractive therapeutic target for the prevention of MASLD [18]. Increased SIRT1 suppresses CD36 expression and prevents high-fat diet (HFD)-induced hepatic steatosis [16]. SIRT1 deacetylates a number of proteins, including histone H3 of CD36 promoter [14,15].

In this study, we investigated the role of TMEM135 on FA importer under hepatic steatosis conditions using *in vivo*, *ex vivo*, and *in vitro* experimental models. Our results suggest that the reduction in intracellular lipid accumulation under TMEM135 depletion is closely linked to the inhibition of lipid import regulated by CD36 in a SIRT1-dependent manner. These findings propose that TMEM135 might be a promising candidate for the treatment of hepatic steatosis.

2. MATERIALS AND METHODS

2.1. Animal

TMEM135 knockout (TMEM135KO) mice were generated by Asan Medical Center (Seoul, Korea) using CRISPER-Cas9 technology. Two sgRNA sequences were sgRNA1: TGTACATTACTTTCTTCTGC and sgRNA2: CCAGTCCGCCTCCTTCCTGA. Pups of wild type (WT), TMEM135KO, and heterozygous were obtained by mating heterozygous TMEM135KO male and female mice, and further verified by genotyping. Primer sequences used for genotyping were 5′-GTTAGTCTTTCACACGCGCT-3′ and 5′-GTTTCCATTTCAACAAAGCAAATTC-3'. Litter mate male mice of WT and TMEM135KO at age of 8-weeks were included in the study. Mice were housed at 22 °C and maintained at 12 h light/dark cycle. WT and TMEM135KO mice were randomly divided into two groups. One group of WT and TMEM135KO mice was fed a normal chow diet (NCD, 10% kcal from fat, #D12450B, Research Diets Inc., New Brunswick, NJ, USA) and the other group was fed a high-fat diet (HFD, 60% kcal from fat, #D12492, Research Diets Inc.) for 22 weeks. All procedures involving mice experiments were conducted according to the guidelines for The Care and Use of Laboratory Animals approved by Gwangju Institute of Science and Technology (GIST), Korea. On the day of sacrifice, mice were fasted for 12 h and anesthetized. The liver was harvested, snap frozen in liquid nitrogen, and then stored at −80 °C until used.

2.2. Isolation and culture of the primary hepatocytes

Primary hepatocytes were isolated from the livers of WT and TMEM135KO mice at age of 8-weeks as described previously [19] with some modifications. Isolated hepatocytes were cultured in William *E. media* (#A1217601, Gibco, Grand Island, NY, USA). They were allowed to grow for 12 h, then treated with or without 150 μM of FFA for 12 h.

2.3. Cell culture

Mouse hepatocyte cell line, AML12, was purchased from American Type Culture Collection (#CRI-2254, ATCC, Manassas, VA, USA). Cells were cultured in Dulbecco's modified Eagle's medium (DMEM; Gibco, Carlsbad, CA, USA) supplemented with 10% fetal bovine serum (FBS; Gibco, Carlsbad, CA, USA) and 1% penicillin-streptomycin (Gibco, Carlsbad, CA, USA). After 16 h of seeding, cells were treated with or without 150 μM of FFA for 12 h.

2.4. Generation of stable cell lines

Lentivirus transfection (#631276, Takara Bio, CA, USA) method as mentioned by the manufacturer's protocol was followed to generate stable cells with TMEM135 depletion (sh-TMEM135) using shRNA oligos targeting TMEM135 into pLV-[shRNA]-EGFP: T2A: puro-U6>mTMEM135 [shRNA#1]. The shRNA sequence targeting TMEM135 is 5′-TAGAAAGGCGTTGCTTAATAA-3'. shRNA sequence 5′-CCTAAGGTTAAGTCGCCCTCG-3′ in pLV-[shRNA]-EGFP: T2A: puro-U6>sh-Scramble was used for scramble. shRNA was designed and ordered from VectorBuilder. Briefly, pLV-shRNA plasmid was co-transfected with lentivirus packing plasmid into HEK293T cells. Lentiviral supernatant was harvested from HEK293T cells after 48 h of transfection. Supernatant was mixed with 8 μg/ml polybrene (TR-1003-G, Sigma—Aldrich, St. Louis, MO, USA) to increase the transfection efficiency. After 48 h of transfection, cells were selected in 10 μg/ml puromycin (P4512, Sigma—Aldrich, St. Louis, MO, USA) for 3 weeks. The media with puromycin was replenished every 3 days.

2.5. Reagents and antibodies

Sodium palmitate (#P9767), sodium oleate (#07501), and Oil Red O solution (#01391) were purchased from Sigma—Aldrich (St. Louis, MO, USA). CD36 antibody (#NB400-144) and FSP27 (#NB100-430) were bought from Novus Biological (Minneapolis, MN, USA). Anti-PPAR-γ (#2443S), anti-SIRT1 (#9475 and #2028S), anti-SIRT2 (#12650), anti-SIRT3 (#5490), anti-SIRT4 (#69786), anti-SIRT5 (#8782), anti-SIRT6 (#12486), anti-SIRT7 (#5360) and anti-MYC-tag (#2278S) were obtained from Cell Signaling Technology (Beverly, MA, USA). TG assay kit (ab65336) was purchased from Abcam (Abcam, Cambridge, MA, USA). Anti-PLIN2 (15294-1-AP) was bought from Proteintech (Rosemont, IL 6008, USA). HRP Conjugated-Beta actin (#Sc-47778) from Santa Cruz Biotechnology (Dallas, TX, USA), HRP conjugated goat anti-mouse (A90—131P0) and HRP conjugated goat anti-rabbit (#A120—101P) were obtained from Bethyl Laboratories (Montgomery, TX, USA).

2.6. Preparation of free fatty acid (FFA)

Sodium palmitate and sodium oleate powder were weighted and mixed with 150 mM sodium chloride solution separately. Sodium palmitate and sodium oleate were heated at 70 °C and 60 °C, respectively. Then, the solution was mixed for 1 h with fatty acid-free bovine serum albumin (BSA) solution prepared in 150 mM NaCl at 37—40 °C for conjugating fatty acids to BSA. A mixture of palmitic and oleic acid (1:2) was used as FFA. FFA was aliquoted and stored at −20 °C until used.

2.7. Oil Red O (ORO) staining and lipid droplet (LD) quantification

Staining for LDs was performed using ORO solution as the manufacturer's instruction. Cell's nuclei were stained with DAPI. For liver tissue sections, nuclei were stained with Mayer's hematoxylin solution. Images were acquired using a microscope. Quantification of LD size, number, and area was done using ImageJ software [20].

2.8. Plasmids

The plasmid pCMV-TMEM135-myc encoding full-length versions of wild-type mouse TMEM135 followed by five tandem copies of a c-Myc epitome tag (EQKLISEEDL), as mentioned earlier, was used [3]. pcDNA3.1 was used as a control. Plasmid was transfected by using JetOPTIMUS (#101000006, Polyplus) as mentioned by the

manufacturer's protocol. After 12 h of transfection, cells were treated with FFA for 12 h and harvested for further analysis.

2.9. Immunofluorescence staining

Cells were grown on coverslips. As confluency reached around 70%, cells were transfected with TMEM135-myc or control plasmid. After 12 h of transfection, cells were treated with FFA for 12 h and then fixed with 4% paraformaldehyde for 20 min at room temperature. Cells were rinsed three times with PBS, permeabilized with 0.25% TritonX-100 for 5 min, and followed by blocking with 3% BSA for 1 h at room temperature. Cells were incubated with primary antibody overnight. Next, cells were rinsed three times with PBS and incubated with secondary antibodies (1:500) for 1 h. Nucleus was stained with DAPI. Finally, samples were examined under microscope. Image J software was used to quantify the fluorescence intensity.

2.10. FA uptake assay

The stable cell lines, sh-Scramble and sh-TMEM135, were tagged with EGFP. EGFP-tagged sh-RNA cells interfere with the green fluorescence of BODIPY-Palmitate staining during the fine visualization of lipid import. To avoid this issue, we used, si-Control and si-TMEM135, AML12 cells specifically for performing the BODIPY-Palmitate assay. BODIPY-Palmitate (26749, Cayman chemical company, Michigan 48108, USA) was mixed with 1% FFA-free BSA and treated to cells at concentration of 1 μM for 1 h at 37 °C. BSA was used as a control. BSA treatment was used as a control. Then, cells were immediately washed three times with cold PBS. DAPI staining was performed and washed three time with cold PBS. Finally, coverslip was mounted on clean glass slides and fluorescent images were obtained under microscope.

2.11. RNA interference

Procedure followed INTERFERin (#101000028, Polyplus) *in vitro* short interfering RNA (siRNA) transfection reagent protocol from the manufacture. siControl (SN-1003), siTMEM135, and siSIRT1 were purchased from Bioneer (Daejeon, Korea). Double depletion was carried out in sh-TMEM135 cells using siRNA targeting SIRT1. siRNA sequences were as follows: siSIRT1 are 5′-CCCUGUAAAGCUUUCAGAA-3′ and 3′-UUCUGAAAGCUUUACAGGG-5'; siTMEM135 are 5′-UACAAACGUUUUCAUA-3′ and 3′-UAUGAAACCCACGUUUGUA-5'. After 48 h of transfection, cells were treated with FFA for 12 h and collected for further analysis.

2.12. EX-527 treatment

Cells were seeded in 6 cm plate and maintained until they reached 50% of confluency. Then, cells were pretreated with 10 μM EX-527 (2780, TOCRIS, Bristol, UK) or DMSO as a vehicle for 24 h and followed by 12 h of FFA treatment.

2.13. Histology

Cryosection of tissues was prepared by incubating with sucrose 15% and 30%, embedded in OCT, frozen by dry ice for 30 min, and stored at −80 °C. Tissue was sectioned in 8 μm thickness and ORO staining was performed as the manufacturer's instructions described above. Immunohistochemical stain of CD36 was performed from paraffin-embedded liver tissues. Tissues fixed in 10% neutral buffer formalin was sectioned into 5 μm thickness. Deparaffinization of slides was done by heating slide at 60 °C for 15 s. Slides were kept in xylene and then in a series of ethanol 100%, 95% and 70%, and then finally washed with distilled water. Blocking of endogenous peroxides was achieved by incubating slides in 3% H_2O_2 solution for 10 min. Slides were washed in PBS for 5 min thrice. Antigen retrieval was performed by heating slide in citrate buffer for 10 min at 97 °C, and blocking was done for 1 h in 1% BSA containing PBS. Again, slides were washed with PBS for 5 min thrice. Primary antibody was incubated for 1 h at 37 °C and unbound antibody was washed thrice with PBS-T for 5 min. Secondary antibody in GBI kit was incubated for 1 h at room temperature. After wash unbound antibody, then slides were incubated in DAB for 1 min, washed with PBS for 5 min thrice, and counterstained with Mayer's hematoxylin for 1 min. Image was taken using OLYMPUS BX-51 and analyzed by image J software.

2.14. Triglyceride (TG) measurement

Hepatic and intracellular TG levels were determined using TG assay kit (ab65336, Abcam, Cambridge, MA, USA) according to the manufacturer's instruction. Briefly, cells were harvested and washed with cold PBS. The pellet was homogenized in 1 ml of 5% NP40. The homogenate was heated at 80 °C for 2 min and cooled at room temperature. After centrifugation for 2 min, the clear supernatant was transferred to a new EP tube. Protein concentration was measured by Bradford method. After normalization to protein concentration, TG concentration was calculated by reading OD at 570 nm. Similarly, for liver tissue, 100 mg of liver tissue was homogenized in 5% NP40 and followed the similar procedures as mentioned before.

2.15. Diacylglycerol (DAG) measurement

Intracellular DAG levels were determined using DAG assay kit (ab242293, Abcam, Cambridge, MA, USA) according to the manufacturer's instruction. Briefly, cells were harvested and washed with cold PBS. The pellet was resuspended in 1 ml of cold PBS. Then, 1 ml of methanol, 2.25 ml of 1 M NaCl and 2.5 ml of chloroform were added to the sample. The sample was vortex well and centrifuged at 1500 g for 10 min. The upper aqueous phase was discarded and the lower chloroform phase was washed twice with pre-equilibrated upper phase mentioned in manufacturer's protocol. After the final wash, lower organic phase was carefully collected into a glass vial. This lower phase was completely dried in a stream of nitrogen gas. Finally, 50 μl of assay buffer was added and DAG concentration was measured by fluorometric method at excitation in 530—560 nm and emission in 585—595 nm.

2.16. RT-qPCR

Total RNA from liver tissue and cells were prepared by TRIzol reagent (#15596018, Invitrogen, Carlsbad, USA) according to the manufacturer's instruction. A reverse transcription kit (#73201, HK Genomics, Korea) was used to transcribe cDNA. Real-time qPCR was performed with cDNA template using a light cycler system with SYBR green PCR master mix (#4309155, Applied Biosystems, Austin, TX, USA). Primer sequences were listed in the Supplementary table 1 and 36B4was used as an internal control.

2.17. Western blot analysis

Liver tissues and cells were homogenized in RIPA lysis buffer (RC2002-050-00, Biosesang, Seoul, Korea) mixed with 1X protease phosphatase inhibitor cocktail (#1861281, Thermo Scientific, USA). Protein lysate was kept in ice for 15 min and centrifuged at 14000×*g* for 10 min at 4 °C to collect supernatant. Protein concentration was measured by Bradford method (#5000006, BIO-RAD, USA). Protein was mixed with SDS, heated at 97 °C for 5 min, and subjected to SDS-PAGE. Antibody-targeted proteins were visualized using Western blot detection kit (#LF-QC0103, Abfrontier, Seoul, Korea).

2.18. SIRT1 activity assay

SIRT1 activity was measured by SIRT1 activity kit (ab156065, Cambridge, MA, USA) as mentioned by the manufacture's instruction. Fluorescent intensity was measured at 1 min interval for 60 min using CLARIOstar plus microplate reader (BMG LabTech, Germany) at 350 nm excitation and 460 nm emission.

2.19. Metabolomics

Liver samples from WT and TMEM135KO mice fed with either NCD or HFD were collected and sent to Metabolon Inc. (Durham, NC, USA) (N = 6/group) for untargeted metabolite profiling, including NAD^+, NADH, and ceramide analysis [21]. Briefly, samples were extracted and split into equal parts for by liquid chromatography/tandem mass spectrometry (LC/MS/MS). Proprietary software was used to match ions to an in-house library of standards for metabolite identification and for metabolite quantitation by peak area integration. Statistical analysis was performed on natural log-transformed data. For comparison of metabolites in the heatmap, normalized data were converted to z-score.

2.20. Statistical analysis

Statistical analysis was performed using GraphPad Prism version 9.0 (San Diego, CA, USA). Student's t-test and ANOVA were performed as mentioned in the respective figures. Tukey HSD post-hoc test was conducted after ANOVA analysis. Statistical significance was set at a p-value <0.05.

3. RESULTS

3.1. TMEM135 depletion alleviates lipid accumulation in the liver of HFD mice and FFA treated cells

To investigate the role of TMEM135 depletion on lipid accumulation, we performed *in vivo*, *ex vivo* and *in vitro* experiments. TMEM135 expression in mouse liver and knock down cells was confirmed by measuring mRNA expression (Supplementary Figure. S1). The liver of HFD-fed WT mice demonstrated an increased lipid accumulation shown as lipid droplets (LDs), while that of TMEM135KO mice showed less LDs even in HFD conditions (Figure 1A). Consistently, expression of LD-associated

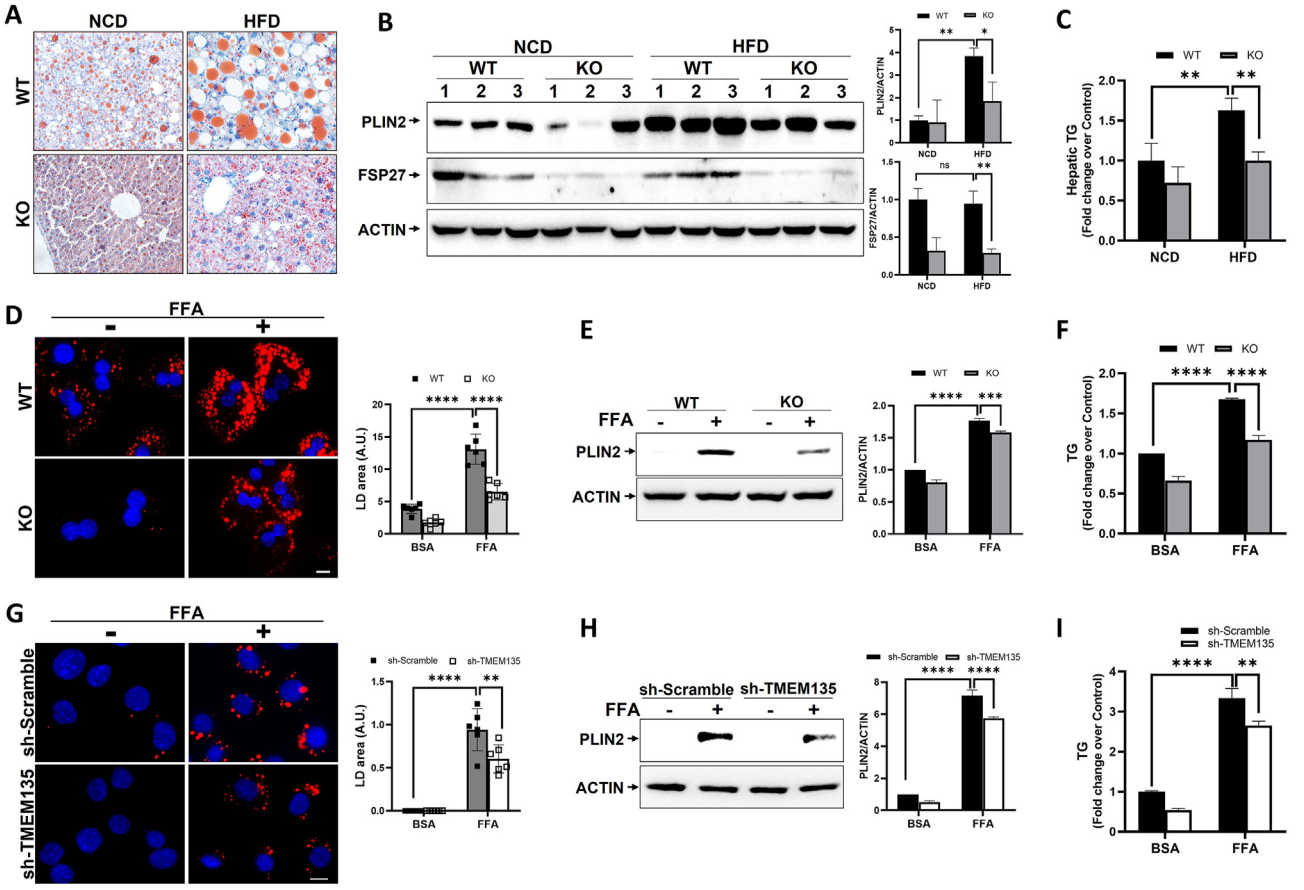

Figure 1: Depletion of TMEM135 decreases lipid accumulation in the liver of HFD mice and FFA-treated primary hepatocytes and AML12 cells. (A–C) WT and TMEM135KO mice were fed either NCD or HFD for 22 weeks (n = 6 per group). (A) Oil Red O staining of liver tissue section (Original magnification x100). (B) Immunoblots and densitometry for PLIN2, FSP27, and β-actin from the liver tissue of mice. Data represent mean ± SD, $^{**}p < 0.01$, $^{*}p < 0.05$, Two-way ANOVA. (C) Hepatic TG levels. Data represent mean ± SD, $^{**}p < 0.01$, Two-way ANOVA. (D–F) Primary hepatocytes were isolated from the livers of WT and TMEM135KO mice and treated with FFA for 12 h. (D) Oil Red O staining and quantification of LD area (Original magnification x40, scale bar 20 μm). More than 100 cells per group in each experiment were measured. Data represent mean ± SD, $^{****}p < 0.0001$, Two-way ANOVA. (E) Immunoblots and densitometry for PLIN2 and β-actin. Data represent mean ± SD, $^{****}p < 0.0001$, $^{***}p < 0.001$, Two-way ANOVA. (F) Quantification of TG levels. Data represent mean ± SD, $^{****}p < 0.0001$, Two-way ANOVA. (G–I) sh-Scramble and sh-TMEM135 cells were treated with FFA for 12 h. (G) Oil Red O staining and quantification of LD area (Original magnification x100, scale bar 20 μm). More than 100 cells per group in each experiment were measured. Data represent mean ± SD, $^{****}p < 0.0001$, $^{**}p < 0.01$, Two-way ANOVA. (H) Immunoblots and densitometry for PLIN2 and β-actin. Data represent mean ± SD, $^{****}p < 0.0001$, Two-way ANOVA. (I) Quantification of TG levels. Data represent mean ± SD, $^{****}p < 0.0001$, $^{**}p < 0.01$, Two-way ANOVA.

proteins [22,23], including PLIN2 and FSP27, was attenuated in the liver of TMEM135KO mice compared to that of WT mice under both NCD and HFD-fed conditions (Figure 1B). Though, PLIN2 expression markedly increased by HFD in both WT and TMEM135KO mice, FSP27 expression did not show any notable change in the liver of HFD-fed TMEM135KO mice (Figure 1B). Next, we measured hepatic TG levels in the mice to confirm the difference in lipid accumulation between WT and TMEM135KO mice. TG accumulation was significantly elevated in the liver of HFD-fed WT mice (Figure 1C). In contrast, TG levels in TMEM135KO mice remained unchanged by HFD feeding, which was almost similar to that under the NCD condition (Figure 1C). We also analyzed the hepatic ceramide levels in WT and TMEM135KO mice (Supplementary Figure. S2). However, various types of ceramides were not changed between WT and TMEM135KO mice, ceramide (d18:1/17:0, d17:1/18:0) was significantly decreased in TMEM135KO mice liver compared to WT, regardless of diet conditions (Supplementary Figure S2 G). Ceramide (d18:1/16:0(2OH)) tended to reduce in WT mice liver under HFD conditions (Supplementary Figure S2 C).

Next, primary hepatocytes were maintained with or without FFA to mimic *in vivo* HFD conditions. ORO staining and LD area quantification results showed that FFA treated primary hepatocytes from TMEM135KO mice had significantly reduced LD accumulation compared to WT (Figure 1D). Furthermore, we measured the number and size of LDs in primary hepatocytes. The number of LDs in primary hepatocytes from TMEM135KO mice was significantly decreased compared to WT mice under FFA treatment (Supplementary Figure S3 A). The average number of LDs per cell was almost 50% less in the primary hepatocytes from TMEM135KO mice compared to WT mice under FFA treatment (Supplementary Figure S3 A). In addition, LD size was smaller in the primary hepatocytes from TMEM135KO mice treated with FFA, while the primary hepatocytes from WT mice were rich in larger LDs (Supplementary Figure S3 B). Approximately, 50% of LDs in the primary hepatocytes from TMEM135KO mice was below 2 μm in diameter and only 20% of LDs was above 3 μm. However, only 22% of LDs in the primary hepatocytes from WT mice was below 2 μm in diameter and 50% of LDs was above 3 μm. The difference in LD accumulation between the primary hepatocytes from WT and TMEM135KO mice was further confirmed by measuring the protein expression of PLIN2. A marked increase in PLIN2 expression by FFA treatment in the primary hepatocytes from WT mice was attenuated in TMEM135 KO mice (Figure 1E). Consistently, primary hepatocytes from TMEM35KO mice showed a significant decrease in TG levels compared to WT mice under both BSA and FFA treatment conditions (Figure 1F). We also demonstrated the effect of TMEM135 depletion on lipid accumulation in AML12 cells, demonstrating that FFA treatment led to a significant reduction in ORO staining and LD area in sh-TMEM135 cells compared to sh-Scramble (Figure 1G). Consistent with primary hepatocytes, sh-TMEM135 cells treated with FFA had reduced LD numbers (Supplementary Figure S3 C). LDs in sh-TMEM135 cells treated with FFA were smaller, whereas LDs in sh-Scramble cells were larger (Supplementary Figure S3 D). Additionally, PLIN2 expression by FFA treatment was augmented in sh-Scramble cells which was markedly attenuated in sh-TMEM135 cells (Figure 1H). sh-TMEM135 cells showed significantly lower TG and diacylglycerol (DAG) levels compared to sh-Scramble cells under FFA treatment, further confirming that lipid storage was reduced in the TMEM135-deficient *in vitro* experimental model (Figure 1I and Supplementary Figure S4 A). Collectively, these observations clearly indicate that TMEM135 may contribute to lipid accumulation, which was significantly suppressed in the liver and the primary hepatocytes of TMEM135KO mice, and sh-TMEM135 AML 12 cells.

3.2. TMEM135 overexpression increases lipid accumulation in FFA treated AML12 cells

Next, to observe the effect of TMEM135 overexpression on lipid accumulation, TMEM135-myc was transfected to AML12 cells for 24 h and followed by FFA treatment for 12 h. Expression of PLIN2 significantly increased by the addition of FFA in both control and TMEM135-myc cells (Figure 2A). However, overexpression of TMEM135 drove more expression of PLIN2 compared to control cells in the presence of FFA. In addition, TG level which was significantly increased by FFA treatment, further augmented in TMEM135-myc cells (Figure 2B). Similarly, FFA treatment significantly increased DAG levels in TMEM135-myc cells compared to control cells (Supplementary Figure S4 B). In TMEM135-myc cells, fluorescence intensity of PLIN2 significantly increased in the presence of FFA compared to control cells (Figure 2C—D). These results suggest that TMEM135 modulates lipid accumulation in the liver and hepatocytes of mice.

3.3. TMEM135 depletion suppresses CD36 expression in the liver of HFD mice and FFA treated cells

Next, we measured the expression of proteins and genes involved in lipid uptake to determine whether the reduced LD accumulation under both TMEM135 deficiency and depletion conditions was due to decreased FFA uptake. CD36, which facilitates the transport of long-chain fatty acids (LCFAs) [8,13], significantly increased in the immunohistochemical staining of the liver of HFD-fed WT mice, whereas that clearly disappeared in TMEM135KO mice (Figure 3A). In parallel, we verified that the protein expression of CD36 markedly upregulated only in the liver of HFD-fed WT mice but not in HFD-fed TMEM135KO mice (Figure 3B). Similarly, protein expression of PPAR-γ, a well-known upstream regulator of CD36, was also increased only in the liver of HFD-fed WT mice compared to NCD-fed WT mice (Figure 3B). Besides *ppar-γ,* we also analyzed the mRNA expression of *lxr* and *pxr*, which are known to regulate CD36 expression [24]. As expected, mRNA expression of *ppar-γ*, *lxr*, *pxr*, and *cd36* was significantly upregulated in the liver of HFD-fed WT mice (Supplementary Figure S5 A-D). However, the protein expression of LXR and PXR between WT and TMEM135KO mice was not different (Supplementary Figure S6). To confirm whether lipid import was solely through CD36 or not, we also measured mRNA expression of other lipid importers, including *fatp2* and *fatp5*, in the liver tissue. There was no difference in their mRNA expression levels (Supplementary Figure S7 A-B).

In consistent with *in vivo* data, the expression of CD36 markedly increased in the primary hepatocytes from WT mice in the presence of FFA, however, it was not obvious in the primary hepatocytes from TMEM135KO mice (Figure 3C). We also tested CD36 protein expression in FFA treated sh-Scramble and sh-TMEM135 cells in a time dependent manner. CD36 expression increased after 15 min of FFA treatment in both cells (Figure 3D). CD36 persisted up to 12 h of FFA treatment in sh-Scramble cells, while that began to markedly reduce in sh-TMEM135 cells after 30 min and completely disappeared after 2 h (Figure 3D). In contrast, TMEM135 overexpression was sufficient to increase CD36 protein expression in AML12 cells, irrespective of FFA treatment (Figure 3E).

Next, to confirm whether lipid import might have altered under TMEM135 depletion, we measured lipid import into cells using BODIPY-Palmitate, a green fluorescence tagged palmitic acid. The intensity of BODIPY-Palmitate increased in siControl cells compared to siTMEM135 transfected cells with statistical significance (Figure 3F). Collectively, these data demonstrate that TMEM135 regulates lipid uptake into cells through CD36 expression in experimental models of *in vivo, ex vivo,* and *in vitro*.

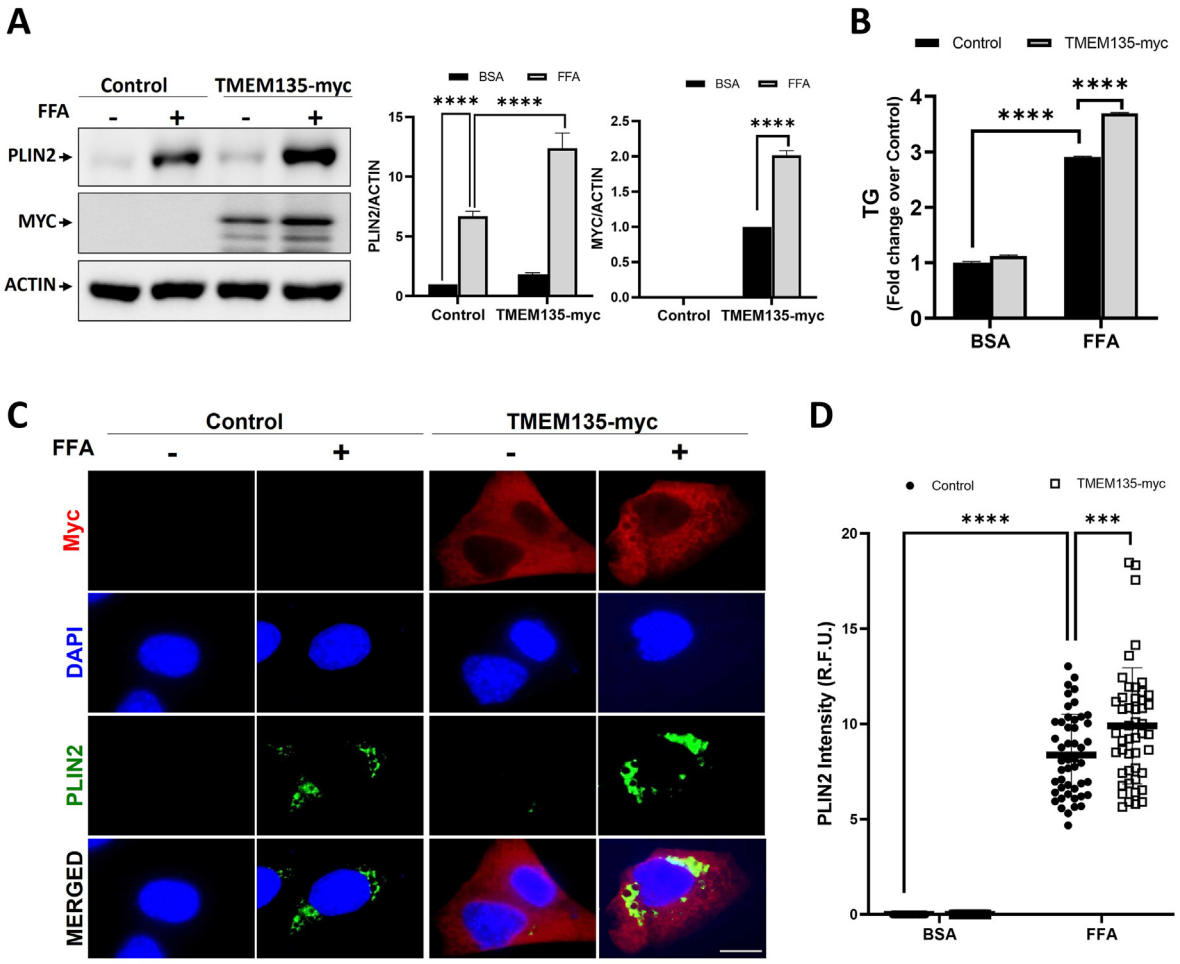

Figure 2: TMEM135 overexpression exacerbates lipid accumulation in FFA-treated AML12 cells. (A—D) AML12 cells overexpressed for TMEM135 were treated with FFA for 12 h (n = 6 per group). (A) Immunoblots and densitometry for PLIN2 and β-actin. Data represent mean ± SD, ****p < 0.0001, Two-way ANOVA. (B) Quantification of TG levels. Data represent mean ± SD, ****p < 0.0001, Two-way ANOVA. (C) Immunofluorescence staining for PLIN2 (Original magnification x100, scale bar 20 μm). (D) Quantification of fluorescence intensity of PLIN2. Data represent mean ± SD, ****p < 0.0001, ***p < 0.001, Two-way ANOVA.

3.4. TMEM135 depletion inhibits lipid accumulation through regulation of CD36 expression in a SIRT1-dependent manner in the liver of HFD mice and FFA treated cells

To identify the possible regulator of CD36 under TMEM135 depletion, we investigated whether CD36 expression could be regulated though SIRT1 [14,15]. Among SIRT family proteins, from SIRT1 to SIRT7, only SIRT1 prominently upregulated in the liver tissue of HFD-fed TMEM135KO mice (Figure 4A). In addition, NAD^+/NADH ratio significantly increased in the liver tissue of TMEM135KO mice compared to WT (Figure 4B). However, there were no significant differences in SIRT1 protein as well as NAD^+/NADH ratio in WT mice irrespective of diets (Figure 4A—B). Consistent with *in vivo* data, SIRT1 expression significantly increased in the primary hepatocytes from TMEM135KO mice with FFA treatment (Figure 4C). Likewise, SIRT1 significantly increased in sh-TMEM135 cells treated with FFA (Figure 4D). However, TMEM135 overexpression markedly reduced SIRT1 expression regardless of FFA treatment (Figure 4E).

To confirm whether CD36 was regulated by SIRT1 in TMEM135 depleted condition, SIRT1 was suppressed with either siRNA or SIRT1 inhibitor EX-527, respectively. Consistent with Figure 3D, FFA treatment increased the protein expression of CD36 only in sh-Scramble cells, but not in sh-TMEM135 (Figure 5A). In addition, PLIN2 expression was significantly higher in sh-Scramble cells compared to sh-TMEM135 under FFA treatment (Figure 5A). However, SIRT1 protein suppression by siSIRT1 transfection in sh-TMEM135 cells increased CD36 protein expression (Figure 5A). PLIN2 expression under FFA treatment was elevated by siSIRT1 transfection in sh-TMEM135 cells and was comparable to that in FFA-treated sh-Scramble cells (Figure 5A). siSIRT1 transfection significantly increased TG levels in sh-TMEM135 cells similar to sh-Scramble cells under FFA treatment (Figure 5B). In contrast, siSIRT1 transfection did not further increase the expression of CD36 and PLIN2 in sh-Scramble cells under FFA treatment (Figure 5A). However, TG levels in sh-Scramble cells tended to increase with siSIRT1 transfection under FFA treatment, and it was also higher than siSIRT1 transfected sh-TMEM135 cell under FFA treatment (Figure 5B). Moreover, FFA treatment increased SIRT1 activity in sh-TMEM135 cells, which was attenuated by siSIRT1 transfection. In contrast, FFA treatment did not result in any detectable change in SIRT1 activity in sh-Scramble cells (Figure 5C).

Next, we also verified the effect of EX-527, a SIRT1 activity inhibitor, on CD36 expression and TG accumulation in sh-TMEM135 cells (Figure 5D—E). Treatment with EX-527 increased CD36 expression

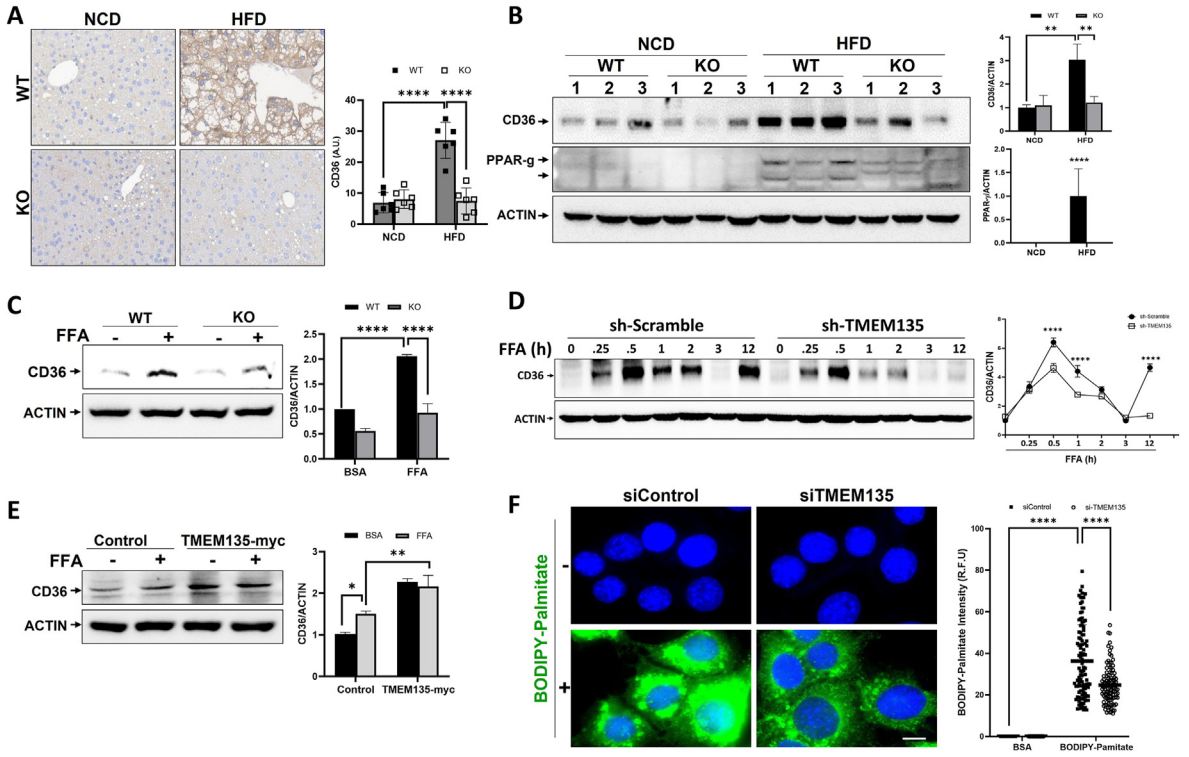

Figure 3: Depletion of TMEM135 decreases CD36 expression in the liver of HFD mice and FFA-treated primary hepatocytes and AML12 cells. (A—B) Mice were fed either NCD or HFD for 22 weeks (n = 6 per group). (A) Immunostaining for CD36 and quantification (Original magnification 100×, scale bar 20 μm). Data represent mean ± SD, ****p < 0.0001, Two-way ANOVA. (B) Immunoblots and densitometry for CD36, PPAR-γ and β-actin. Data represent mean ± SD, ****p < 0.0001, **p < 0.01, Two-way ANOVA (C) Immunoblots and densitometry for CD36 and β-actin in the primary hepatocytes treated with FFA for 12 h. Data represent mean ± SD, ****p < 0.0001, Two-way ANOVA. (D) Immunoblots and densitometry for CD36 and β-actin in sh-Scramble and sh-TMEM135 cells treated with FFA for 12 h. Data represent mean ± SD, ****p < 0.0001, Two-way ANOVA (E) Immunoblots and densitometry for CD36 and β-actin in TMEM135 overexpressed cells treated with FFA for 12 h. Data represent mean ± SD, **p < 0.01, *p < 0.05, Two-way ANOVA. (F) Immunofluorescence staining and quantification for BODIPY-Palmitate in si-Control and si-TMEM135 cells (Original magnification x100, scale bar 20 μm). Data represent mean ± SD, ****p < 0.0001, Two-way ANOVA.

similarly to siSIRT1 transfection in sh-TMEM135 cells (Figure 5D). Accordingly, EX-527 treatment in sh-TMEM135 cells increased PLIN2 expression and TG accumulation in the presence of FFA (Figure 5D—E). However, the protein expression of CD36 and PLIN2 was not changed in sh-Scramble cells by EX-527 treatment in the presence of FFA. EX-527 treatment with FFA did not induce any detectable changes in TG accumulation in sh-Scramble cells. Taken together, TMEM135 depletion increases NAD^+/NADH ratio, which further induces SIRT1 that inhibits CD36 expression and lipid import (Figure 5F).

4. DISCUSSION

Previous studies relate the role of TMEM135 in peroxisome abundance [1], mitochondrial dynamics [4] and lipid metabolism [1,2]. There is controversy among studies regarding the role of TMEM135 in lipid metabolism [1,2,5,25]. On one hand, TMEM135 mutant (TMEM135-$^{FUN025/FUN025}$) has been reported to increase the gene expression relating to cholesterol metabolism, FA metabolism and steroid metabolism along with increased lipid accumulation in the mouse eyecup [5]. In addition, siRNA-mediated knockdown of TMEM135 in HepG2 cells resulted in increased basal TG accumulation [26]. Similarly, reduced TMEM135 expression has been reported in the abdominal subcutaneous white adipose tissue of obese females [25]. On the other hand, TMEM135$^{FUN025/FUN025}$ has been shown to reduce hepatic lipid accumulation in Lep$^{ob/ob}$ mice with an increase in peroxisomal proteins, including those involved in FAO [1]. Global TMEM135 transgenic (TG) mice exhibit small-sized adipocytes and absence of liver fat accumulation even with HFD-feeding [25]. In contrary, the heart of TMEM135TG mice has increased oxidative stress and might trigger ER stress [27]. However, other independent studies have demonstrated that ER stress upregulates CD36, thereby increasing lipid accumulation [28]. So far, the changes in peroxisomal content and mitochondrial dynamics have been reported with lipid accumulation in TMEM135 mutant mice [1,25].

In this study, we addressed the unknown role of TMEM135 in regulating lipid uptake ultimately affecting the cellular lipid contents by *in vivo*, *ex vivo,* and *in vitro* studies. Although, recent studies have established a role of CD36 in FA uptake that serves as a substrate for TG synthesis and the development of steatosis [29,30]. HFD and FFA did not induce CD36 expression under TMEM135 depleted conditions. Besides CD36, we measured mRNA expression of *fatp2* and *fatp5* which are known to be prominent in the liver tissue. It is expected that an increase in FFA flux happens through FATPs in the absence of CD36 [11,31]. We found no significant difference in FATP expression between WT and TMEM135KO mice. However, an increased tendency of *fatp5* mRNA expression in the liver of TMEM135KO mice could also be one of the compensatory mechanisms in the absence of CD36 [11]. TMEM135KO liver showed reduced CD36 and lipid accumulation compared to WT under HFD condition, despite increased tendency of FATP5. Therefore, our study focused on lipid import through CD36. Although we expected complete absence of LDs in sh-TMEM135 cells treated with FFA, we observed increased lipid accumulation compared

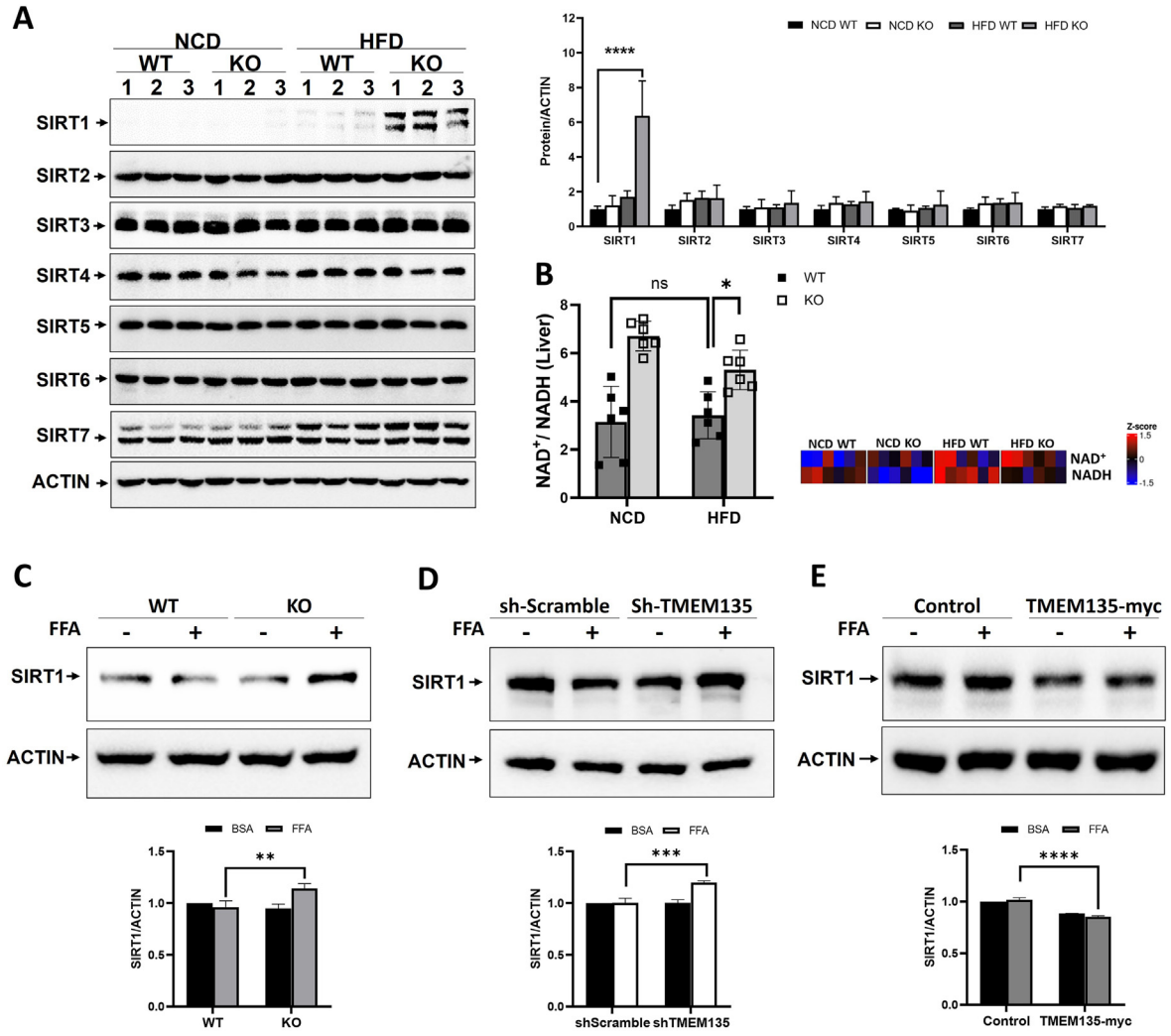

Figure 4: Depletion of TMEM135 increases SIRT1 expression and NAD$^+$/NADH ratio in the liver of HFD mice, and FFA-treated primary hepatocytes and AML12 cells. (A–B) WT and TMEM135KO mice were fed either NCD or HFD for 22 weeks (n = 6 per group). (A) Immunoblots and densitometry for SIRT family proteins and β-actin. Data represent mean ± SD, ****p < 0.0001, Two-way ANOVA. (B) Quantification of NAD$^+$/NADH ratio, and heatmap showing NAD$^+$ and NADH levels from metabolomics. Data represent mean ± SD, *p < 0.05, Two-way ANOVA. (C) Immunoblot and densitometry for SIRT1 and β-actin in the primary hepatocytes from WT and KO treated with FFA for 12 h. Data represent mean ± SD, **p < 0.01, Two-way ANOVA. (D) Immunoblot and densitometry for SIRT1 and β-actin in sh-Scramble and sh-TMEM135 cells treated with FFA for 12 h. Data represent mean ± SD, ***p < 0.001, Two-way ANOVA. (E) Immunoblot and densitometry for SIRT1 and β-actin in TMEM135 overexpressed AML12 cells treated with FFA for 12 h. Data represent mean ± SD, ****p < 0.0001, Two-way ANOVA.

to BSA treatment. An increased lipid in sh-TMEM135 cells could be possibly due to a slight increase in *fatp5* or passive diffusion. These data indicate that among several FA importers present in liver tissue, CD36 expression was specifically affected by TMEM135 depletion. Therefore, we propose that the primary mechanism for reduced lipid accumulation in TMEM135 deficiency may be prevention of FA uptake through downregulation of CD36 expression.

Fatty liver diseases are characterized by the accumulation of neutral lipids inside LD in hepatocytes [32]. Upon HFD, rodents develop fatty liver with an increased expression of PLIN2 and FSP27, similar to patients with MASLD [29,32–36]. However, HFD did not equally increase the expression of these LD proteins, including PLIN2 and FSP27, in the liver tissue of TMEM135KO mice. This is consistent with our hypothesis that in the absence of CD36 expression, lipid may not be taken up as efficiently into the liver of TMEM135KO mice as compared to WT, resulting in reduced lipid accumulation under HFD-fed conditions. Moreover, reduced LD size by blocking FA uptake through CD36 has been demonstrated earlier [37]. As CD36 was expressed only for the initial few hours upon FFA treatment in sh-TMEM135 cells, we assume that both reduced LD size and TG level in TMEM135-depleted cells might be due to limited import of FFA during the fade out of CD36 expression. However, inhibition of lipolysis and lipophagy could also result in the accumulation of larger and smaller LD in the hepatocytes, respectively [38]. Besides, an increase in peroxisomal FAO could be another factor for reduced LD accumulation in TMEM135-depleted cells [1]. In contrary, an increased CD36 expression in TMEM135-overexpressed cells indicates an increased lipid import into cells with an enhanced lipid accumulation, as demonstrated by both increased PLIN2 and TG levels. However, the reduced peroxisomal FAO proteins have been described in the liver of TMEM135TG mice [1]. Surprisingly, FFA treatment facilitated PLIN2 expression under TMEM135 overexpression conditions, suggesting that TMEM135 plays a crucial role in increased lipid accumulation. However, a previous study in *Caenorhabditis elegans* showed that TMEM135-GFP co-localizes with LD

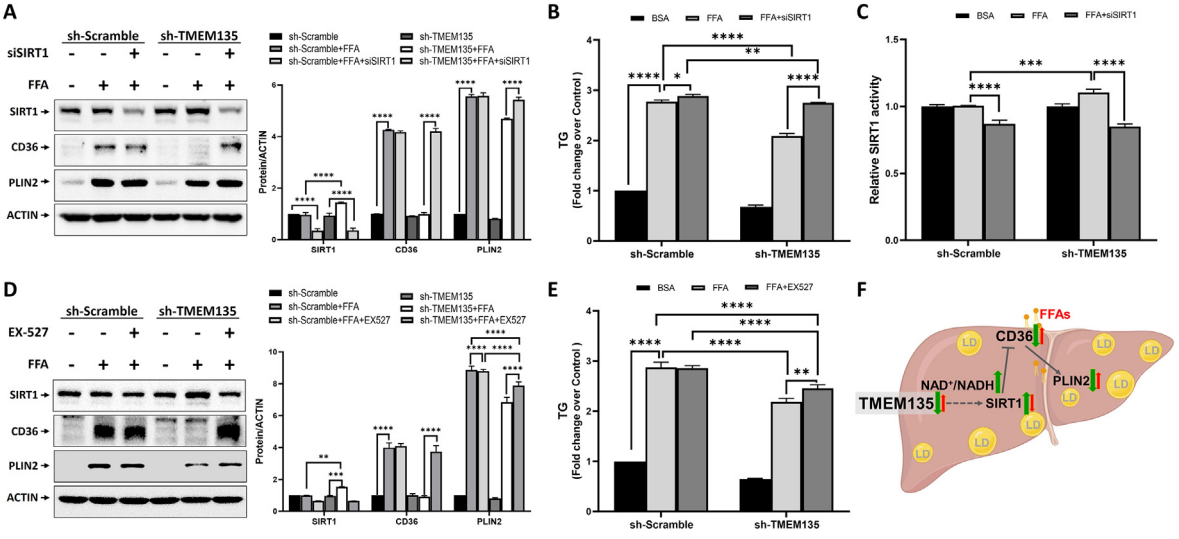

Figure 5: Inhibition of SIRT1 increases lipid import and accumulation through CD36 upregulation in TMEM135-depleted AML12 cells. (A–C) sh-Scramble and sh-TMEM135 cells were transfected with siSIRT1 and then treated with FFA for 12 h (n = 6 per group). (A) Immunoblots and densitometry for SIRT1, CD36, PLIN2 and β-actin. Data represent mean ± SD, ****$p < 0.0001$, Two-way ANOVA. (B) Quantification of TG levels. Data represent mean ± SD, ****$p < 0.0001$, **$p < 0.01$, Two-way ANOVA. (C) Quantification of SIRT1 activity. Data represent mean ± SD, ****$p < 0.0001$, *$p < 0.05$, Two-way ANOVA. (D–E) sh-Scramble and sh-TMEM135 cells were treated with EX-527 in present or absent of FFA treatment. (D) Immunoblot and densitometry for SIRT1, CD36, PLIN2 and β-actin. Data represent mean ± SD, ****$p < 0.0001$, **$p < 0.01$, Two-way ANOVA. (E) Quantification of TG levels. Data represent mean ± SD, ****$p < 0.0001$, **$p < 0.01$, Two-way ANOVA. (F) Proposed mechanism that represents TMEM135 depletion decreases fatty acid import and accumulation in the liver.

without a significant change in lipid accumulation [2]. This difference in observation might be due to different experimental models between *C. elegans* and AML12 hepatocytes.

Provided that lipid metabolism in the liver relies on interplay among various tissues [39], our *ex vivo* and *in vitro* results showed that TMEM135-deficient cells exhibited less lipid accumulation compared to control cells in the presence of FFA. This strongly implies that the reduced lipid accumulation in the liver of TMEM135KO mice may be due to lipid metabolism mediated by intrahepatic interplays between different liver cell types.

Next, we tried to clarify the mechanism by which TMEM135KO prevents lipid import and accumulation. TMEM135 depletion has been reported to increase *sirt3* mRNA expression in HepG2 cells [26]. SIRT1 is known to regulate both PPAR-γ and CD36 [14–16,40]. Therefore, we also investigated the involvement of SIRT proteins in TMEM135KO mice. Upregulated SIRT1 protein expression in liver tissue of HFD-fed TMEM135KO mice could be related to the suppressed expression of PPAR-γ and CD36 [14,40]. Yet, we did not clarify whether SIRT1 regulated CD36 was secondary to PPAR-γ in this study. SIRT1 is known to downregulate CD36 expression by the histone deacetylation of CD36 promoter region [14,15]. Our data suggest that the inability to upregulate SIRT1 expression in HFD-fed WT mice could have failed to inhibit the expression of PPAR-γ and CD36 [14,40]. In addition, NAD^+/NADH ratio, which is known to increase the expression and activity of SIRT1, increased in the liver of TMEM135KO mice [14,41,42]. Though, the ratio was higher also in the liver of NCD-fed TMEM135KO, an increase in SIRT1 was observable only in that of HFD-fed TMEM135KO. We assume that NCD could not induce CD36 expression, thus SIRT1 is not required to be upregulated in the liver of NCD-fed TMEM135KO mice. Besides, CD36 expression and lipid accumulation were increased in autophagy deficient cells, specifically ATG5 knockout dendritic cells [43]. SIRT1 also induces autophagy [44]. We observed that SIRT1 was induced in sh-TMEM135 only after FFA treatment. Therefore, it is possible that the initial degradation of CD36 was suppressed in sh-TMEM135 cells. An increase in SIRT1 after FFA treatment indicates the possibility of autophagic degradation of CD36. However, in this study, we did not detect autophagic degradation of CD36. Likewise, *ex vivo* and *in vitro* studies with FFA in TMEM135 depleted cells demonstrated an increase in SIRT1 expression with suppressed CD36 expression. We hypothesized that TMEM135 depletion might increase the activity of mitochondria complexes I, thus generating NAD^+. An increase in NAD^+/NADH ratio might have upregulated SIRT1 expression and activity [45,46]. However, SIRT1 inhibition by siRNA or EX-527 in TMEM135-depleted cells increased CD36 expression [47]. A decrease in SIRT1 protein expression, either with siSIRT1 or EX-527 treatment, resulted in increased lipid accumulation, which was consistent with previous studies [48–50].

In this study, we expected to observe a similar level of lipid accumulation in shTMEM135 cells co-treated with EX527 and FFA as seen in FFA-treated sh-Scramble cells. However, we observed a smaller increase in TG in sh-TMEM135 cells upon co-treatment. Previous studies have also reported controversial results on the magnitude of lipid accumulation in AML12 cells following the same concentration of EX527 treatment. Several studies have shown that EX527 enhanced TG accumulation to a greater extent when treated with 1 mM FFA for 24 h [50]. However, other studies have reported a smaller increase in TG levels by EX527 when treated with 500 μM PA for 24 h [51]. We treated cells with 150 μM FFA for 12 h. Therefore, the differences in the magnitude of lipid accumulation by EX-527 treatment between the previous studies and ours may be due to the concentrations and duration of FFA treatment.

Moreover, the administration of SIRT1 activator, SRT1720, to HFD mice recovers SIRT1 expression and suppresses CD36 expression accompanied by a decrease in hepatic lipid accumulation [16]. Similar to heterozygous SIRT1KO mice fed with HFD, which showed an increase in both CD36 expression and hepatic lipid accumulation, reduced SIRT1 protein in TMEM135 overexpressed cells failed to suppress CD36 expression [17]. Thus, increased lipid imports in TMEM135 overexpressed cells likely resulted in an increase of lipid accumulation. Therefore, it is reasonable to speculate that an increase in SIRT1 under TMEM135 depleted conditions attenuates CD36 expression and

cellular FA uptake upon HFD or FFA treatment. We also expected that siSIRT1 transfection would increase CD36 expression to a great extent than in FFA treated sh-Scramble cells, consistent with the results observed in TMEM135-myc cells. However, it is important to acknowledge the fact that TMEM135-myc cells are influenced not only by reduced SIRT1 protein but also by forced expression of TMEM135 itself. In addition, we assume that the failure of siSIRT1 or EX-527 to elevate CD36 expression in sh-Scramble cells may be due to the already saturated levels of CD36 under FFA treatment. Moreover, an increased TG accumulation without CD36 protein upregulation by siSIRT1 in FFA treated sh-Scramble might be due to altered SIRT1-mediated signaling cascade, such as FAO or de novo lipogenesis, instead of increased lipid import [52].

5. CONCLUSION

Our results demonstrate that TMEM135 regulates hepatic lipid uptake. Either transcriptional deficiency or depletion of TMEM135 reduces the lipid accumulation and TG levels *in vivo* and *in vitro*. In addition, we demonstrate that TMEM135 modulates FFA uptake in liver tissue through SIRT1-mediated downregulation of CD36. Taken together, TMEM135 could be a novel target for preventing lipid uptake in steatosis.

CRediT AUTHORSHIP CONTRIBUTION STATEMENT

Arun Chhetri: Writing — original draft, Visualization, Validation, Resources, Methodology, Investigation, Formal analysis, Data curation, Conceptualization. **Channy Park:** Writing - review and editing, Project administration, Data curation. **Hyunsoo Kim:** Resources, Data curation. **Laxman Manandhar:** Resources, Data curation. **Chagtsalmaa Chuluunbaatar:** Resources, Data curation. **Jaetaek Hwang:** Resources, Data curation. **Xiaofan Wei:** Resources, Data curation. **Gyuho Jang:** Resources. **Batching Chinbold:** Resources. **Hyug Moo Kwon:** Funding acquisition. **Sang-wook Lee:** Resources. **Raekil Park:** Writing — review & editing, Supervision, Resources, Methodology, Investigation, Funding acquisition, Data curation, Conceptualization.

FUNDING SOURCES

This work was supported by the National Research Foundation of Korea (NRF) under grants funded by the Korean government (Grant Nos. 2018R1A5A1024340 and 2022R1A2C3007463), and by a GIST Research Institute (GRI) Grant funded by GIST in 2023.

DATA AVAILABILITY

Data will be made available on request.

ABBREVIATIONS

TMEM135	transmembrane protein 135
TG	triglyceride
LD	lipid droplet
CD36	cluster differentiate 36
SIRT1	Sirtuin 1
sh-TMEM135	short hairpin TMEM135 knock down
siSIRT1	short interfering SIRT1 RNA
HFD	high fat diet
NCD	normal chow diet
FFA	free fatty acid
FA	fatty acid
PLIN2	perilipin 2
PPAR-γ	peroxisome proliferator activated receptor-gamma
LXR	liver X receptor
PXR	pregnane X receptor

ACKNOWLEDGEMENTS

N/A.

DECLARATION OF COMPETING INTEREST

The authors who have taken part in this study declared that they do not have anything to disclose regarding funding or conflict of interest with respect to this manuscript.

APPENDIX A. SUPPLEMENTARY DATA

Supplementary data to this article can be found online at https://doi.org/10.1016/j.molmet.2024.102080.

REFERENCES

[1] Landowski M, Bhute VJ, Grindel S, Haugstad Z, Gyening YK, Tytanic M, et al. Transmembrane protein 135 regulates lipid homeostasis through its role in peroxisomal DHA metabolism. Commun Biol 2023;6(1):8.

[2] Exil VJ, Silva Avila D, Benedetto A, Exil EA, Adams MR, Au C, et al. Stressed-induced TMEM135 protein is part of a conserved genetic network involved in fat storage and longevity regulation in Caenorhabditis elegans. PLoS One 2010;5(12):e14228.

[3] Maharjan Y, Lee JN, Kwak SA, Dutta RK, Park C, Choe SK, et al. TMEM135 regulates primary ciliogenesis through modulation of intracellular cholesterol distribution. EMBO Rep 2020;21(5):e48901.

[4] Lee WH, Higuchi H, Ikeda S, Macke EL, Takimoto T, Pattnaik BR, et al. Mouse Tmem135 mutation reveals a mechanism involving mitochondrial dynamics that leads to age-dependent retinal pathologies. Elife 2016;5.

[5] Landowski M, Bhute VJ, Takimoto T, Grindel S, Shahi PK, Pattnaik BR, et al. A mutation in transmembrane protein 135 impairs lipid metabolism in mouse eyecups. Sci Rep 2022;12(1):756.

[6] Ipsen DH, Lykkesfeldt J, Tveden-Nyborg P. Molecular mechanisms of hepatic lipid accumulation in non-alcoholic fatty liver disease. Cell Mol Life Sci 2018;75(18):3313—27.

[7] Geng Y, Faber KN, de Meijer VE, Blokzijl H, Moshage H, et al. How does hepatic lipid accumulation lead to lipotoxicity in non-alcoholic fatty liver disease? Hepatol Int 2021;15(1):21—35.

[8] Feng Y, Sun W, Sun F, Yin G, Liang P, Chen S, et al. Biological mechanisms and related natural inhibitors of CD36 in nonalcoholic fatty liver. Drug Des Dev Ther 2022;16:3829—45.

[9] Luiken JJ, Chanda D, Nabben M, Neumann D, Glatz JF, et al. Post-translational modifications of CD36 (SR-B2): implications for regulation of myocellular fatty acid uptake. Biochim Biophys Acta 2016;1862(12):2253—8.

[10] Nickerson JG, Alkhateeb H, Benton CR, Lally J, Nickerson J, Han XX, et al. Greater transport efficiencies of the membrane fatty acid transporters FAT/CD36 and FATP4 compared with FABPpm and FATP1 and differential effects on fatty acid esterification and oxidation in rat skeletal muscle. J Biol Chem 2009;284(24):16522—30.

[11] Wilson CG, Tran JL, Erion DM, Vera NB, Febbraio M, Weiss EJ, et al. Hepatocyte-specific disruption of CD36 attenuates fatty liver and improves insulin sensitivity in HFD-fed mice. Endocrinology 2016;157(2):570—85.

[12] Hajri T, Han XX, Bonen A, Abumrad NA. Defective fatty acid uptake modulates insulin responsiveness and metabolic responses to diet in CD36-null mice. J Clin Invest 2002;109(10):1381—9.

[13] He J, Lee JH, Febbraio M, Xie W. The emerging roles of fatty acid translocase/CD36 and the aryl hydrocarbon receptor in fatty liver disease. Exp Biol Med (Maywood) 2011;236(10):1116–21.
[14] Cao Y, Xue Y, Xue L, Jiang X, Wang X, Zhang Z, et al. Hepatic menin recruits SIRT1 to control liver steatosis through histone deacetylation. J Hepatol 2013;59(6):1299–306.
[15] Choi JH, Nam KH, Kim J, Baek MW, Park JE, Park HY, et al. Trichostatin A exacerbates atherosclerosis in low density lipoprotein receptor-deficient mice. Arterioscler Thromb Vasc Biol 2005;25(11):2404–9.
[16] Niu B, He K, Li P, Gong J, Zhu X, Ye S, et al. SIRT1 upregulation protects against liver injury induced by a HFD through inhibiting CD36 and the NF-κB pathway in mouse kupffer cells. Mol Med Rep 2018;18(2):1609–15.
[17] Xu F, Gao Z, Zhang J, Rivera CA, Yin J, Weng J, et al. Lack of SIRT1 (Mammalian Sirtuin 1) activity leads to liver steatosis in the SIRT1+/- mice: a role of lipid mobilization and inflammation. Endocrinology 2010;151(6):2504–14.
[18] Colak Y, Yesil A, Mutlu HH, Caklili OT, Ulasoglu C, Senates E, et al. A potential treatment of non-alcoholic fatty liver disease with SIRT1 activators. J Gastrointestin Liver Dis 2014;23(3):311–9.
[19] Charni-Natan M, Goldstein I. Protocol for primary mouse hepatocyte isolation. STAR Protoc 2020;1(2):100086.
[20] Stuhr NL, Nhan JD, Hammerquist AM, Van Camp B, Reoyo D, Curran SP, et al. Rapid lipid quantification in Caenorhabditis elegans by Oil red O and nile red staining. Bio Protoc 2022;12(5):e4340.
[21] McCall KD, Walter D, Patton A, Thuma JR, Courreges MC, Palczewski G, et al. Anti-inflammatory and therapeutic effects of a novel small-molecule inhibitor of inflammation in a male C57bl/6J mouse model of obesity-induced NAFLD/MAFLD. J Inflamm Res 2023;16:5339–66.
[22] Langhi C, Baldán Á. CIDEC/FSP27 is regulated by peroxisome proliferator-activated receptor alpha and plays a critical role in fasting- and diet-induced hepatosteatosis. Hepatology 2015;61(4):1227–38.
[23] Libby AE, Bales E, Orlicky DJ, McManaman JL. Perilipin-2 deletion impairs hepatic lipid accumulation by interfering with sterol regulatory element-binding protein (SREBP) activation and altering the hepatic lipidome. J Biol Chem 2016;291(46):24231–46.
[24] Zhou J, Febbraio M, Wada T, Zhai Y, Kuruba R, He J, et al. Hepatic fatty acid transporter Cd36 is a common target of LXR, PXR, and PPARgamma in promoting steatosis. Gastroenterology 2008;134(2):556–67.
[25] Hu D, Tan M, Lu D, Kleiboeker B, Liu X, Park H, et al. TMEM135 links peroxisomes to the regulation of brown fat mitochondrial fission and energy homeostasis. Nat Commun 2023;14(1):6099.
[26] Renquist BJ, Madanayake TW, Hennebold JD, Ghimire S, Geisler CE, Xu Y, et al. TMEM135 is an LXR-inducible regulator of peroxisomal metabolism. 2019. p. 334979.
[27] Lewis SA, Takimoto T, Mehrvar S, Higuchi H, Doebley AL, Stokes G, et al. The effect of Tmem135 overexpression on the mouse heart. PLoS One 2018;13(8):e0201986.
[28] Yao S, Miao C, Tian H, Sang H, Yang N, Jiao P, et al. Endoplasmic reticulum stress promotes macrophage-derived foam cell formation by up-regulating cluster of differentiation 36 (CD36) expression. J Biol Chem 2014;289(7):4032–42.
[29] Greco D, Kotronen A, Westerbacka J, Puig O, Arkkila P, Kiviluoto T, et al. Gene expression in human NAFLD. Am J Physiol Gastrointest Liver Physiol 2008;294(5):G1281–7.
[30] Miquilena-Colina ME, Lima-Cabello E, Sánchez-Campos S, García-Mediavilla MV, Fernández-Bermejo M, Lozano-Rodríguez T, et al. Hepatic fatty acid translocase CD36 upregulation is associated with insulin resistance, hyperinsulinaemia and increased steatosis in non-alcoholic steatohepatitis and chronic hepatitis C. Gut 2011;60(10):1394–402.
[31] Clugston RD, Yuen JJ, Hu Y, Abumrad NA, Berk PD, Goldberg IJ, et al. CD36-deficient mice are resistant to alcohol- and high-carbohydrate-induced hepatic steatosis. J Lipid Res 2014;55(2):239–46.
[32] Okumura T. Role of lipid droplet proteins in liver steatosis. J Physiol Biochem 2011;67(4):629–36.
[33] Brasaemle DL, Barber T, Kimmel AR, Londos C. Post-translational regulation of perilipin expression. Stabilization by stored intracellular neutral lipids. J Biol Chem 1997;272(14):9378–87.
[34] Nocetti D, Espinosa A, Pino-De la Fuente F, Sacristán C, Bucarey JL, Ruiz P, et al. Lipid droplets are both highly oxidized and Plin2-covered in hepatocytes of diet-induced obese mice. Appl Physiol Nutr Metabol 2020;45(12):1368–76.
[35] Straub BK, Stoeffel P, Heid H, Zimbelmann R, Schirmacher P, et al. Differential pattern of lipid droplet-associated proteins and de novo perilipin expression in hepatocyte steatogenesis. Hepatology 2008;47(6):1936–46.
[36] Matsusue K, Kusakabe T, Noguchi T, Takiguchi S, Suzuki T, Yamano S, et al. Hepatic steatosis in leptin-deficient mice is promoted by the PPARgamma target gene Fsp27. Cell Metabol 2008;7(4):302–11.
[37] Hao JW, Wang J, Guo H, Zhao YY, Sun HH, Li YF, et al. CD36 facilitates fatty acid uptake by dynamic palmitoylation-regulated endocytosis. Nat Commun 2020;11(1):4765.
[38] Schott MB, Weller SG, Schulze RJ, Krueger EW, Drizyte-Miller K, Casey CA, et al. Lipid droplet size directs lipolysis and lipophagy catabolism in hepatocytes. J Cell Biol 2019;218(10):3320–35.
[39] Bonet ML, Ribot J, Palou A. Lipid metabolism in mammalian tissues and its control by retinoic acid. Biochim Biophys Acta 2012;1821(1):177–89.
[40] Picard F, Kurtev M, Chung N, Topark-Ngarm A, Senawong T, Machado De Oliveira R, et al. Sirt1 promotes fat mobilization in white adipocytes by repressing PPAR-gamma. Nature 2004;429(6993):771–6.
[41] Cantó C, Gerhart-Hines Z, Feige JN, Lagouge M, Noriega L, Milne JC, et al. AMPK regulates energy expenditure by modulating NAD+ metabolism and SIRT1 activity. Nature 2009;458(7241):1056–60.
[42] Pfluger PT, Herranz D, Velasco-Miguel S, Serrano M, Tschöp MH, et al. Sirt1 protects against high-fat diet-induced metabolic damage. Proc Natl Acad Sci U S A 2008;105(28):9793–8.
[43] Oh DS, Lee HK. Autophagy protein ATG5 regulates CD36 expression and anti-tumor MHC class II antigen presentation in dendritic cells. Autophagy 2019;15(12):2091–106.
[44] Huang R, Xu Y, Wan W, Shou X, Qian J, You Z, et al. Deacetylation of nuclear LC3 drives autophagy initiation under starvation. Mol Cell 2015;57(3):456–66.
[45] Ma C, Pi C, Yang Y, Lin L, Shi Y, Li Y, et al. Nampt expression decreases age-related senescence in rat bone marrow mesenchymal stem cells by targeting Sirt1. PLoS One 2017;12(1):e0170930.
[46] Cakir I, Perello M, Lansari O, Messier NJ, Vaslet CA, Nillni EA, et al. Hypothalamic Sirt1 regulates food intake in a rodent model system. PLoS One 2009;4(12):e8322.
[47] He Z, Guo T, Cui Z, Xu J, Wu Z, Yang X, et al. New understanding of Angelica sinensis polysaccharide improving fatty liver: the dual inhibition of lipid synthesis and CD36-mediated lipid uptake and the regulation of alcohol metabolism. Int J Biol Macromol 2022;207:813–25.
[48] Li Q, Tan JX, He Y, Bai F, Li SW, Hou YW, et al. Atractylenolide III ameliorates non-alcoholic fatty liver disease by activating hepatic adiponectin receptor 1-mediated AMPK pathway. Int J Biol Sci 2022;18(4):1594–611.
[49] Yang X, Wei J, He Y, Jing T, Li Y, Xiao Y, et al. SIRT1 inhibition promotes atherosclerosis through impaired autophagy. Oncotarget 2017;8(31):51447–61.
[50] Liu Y, Li Y, Wang J, Yang L, Yu X, Huang P, et al. Salvia-Nelumbinis naturalis improves lipid metabolism of NAFLD by regulating the SIRT1/AMPK signaling pathway. BMC Complement Med Ther 2022;22(1):213.
[51] Yang JW, Zou Y, Chen J, Cui C, Song J, Yang MM, et al. Didymin alleviates metabolic dysfunction-associated fatty liver disease (MAFLD) via the stimulation of Sirt1-mediated lipophagy and mitochondrial biogenesis. J Transl Med 2023;21(1):921.
[52] Hua YQ, Zeng Y, Xu J, Xu XL. Naringenin alleviates nonalcoholic steatohepatitis in middle-aged Apoe(-/-)mice: role of SIRT1. Phytomedicine 2021;81:153412.

